Extracellular Vesicles based STAT3 delivery as innovative therapeutic approach to restore STAT3 signaling deficiency

Ilaria Bettin [a], Martina Brattini [a], Elham Ataie Kachoie [b], Stefano Capaldi [b], Muhammed Ashiq Thalappil [a], Paolo Bernardi [c], Isacco Ferrarini [d], Gregor Fuhrmann [e], Sofia Mariotto [a,*], Elena Butturini [a]

[a] *Department of Neuroscience, Biomedicine and Movement Sciences, Section of Biological Chemistry, University of Verona, Strada Le Grazie, 8, 37134 Verona, Italy*
[b] *Department of Biotechnology, University of Verona, Strada Le Grazie, 15, 37134 Verona, Italy*
[c] *Department of Neuroscience, Biomedicine and Movement Sciences, Section of Human Anatomy, University of Verona, Strada Le Grazie, 8, 37134 Verona, Italy*
[d] *Department of Engineering for Innovation Medicine, Section of Hematology, University of Verona, Verona, Italy*
[e] *Friedrich-Alexander-Universität Erlangen-Nürnberg, Department of Biology, Pharmaceutical Biology, Staudtstr. 5, 91058 Erlangen, Germany*

ARTICLE INFO

ABSTRACT

Extracellular Vesicles (EVs) have been proposed as a promising tool for drug delivery because of their natural ability to cross biological barriers, protect their cargo, and target specific cells. Moreover, EVs are not recognized by the immune system as foreign, reducing the risk of an immune response and enhancing biocompatibility. Herein, we proposed an alternative therapeutic strategy to restore STAT3 signaling exploiting STAT3 loaded EVs. This approach could be useful in the treatment of Autosomal Dominant Hyper-IgE Syndrome (AD-HIES), a rare primary immunodeficiency and multisystem disorder due to the presence of mutations in *STAT3* gene. These mutations alter the signal transduction of STAT3, thereby impeding Th17 CD4$^+$ cell differentiation that leads to the failure of immune response. We set up a simple and versatile method in which EVs were loaded with fully functional STAT3 protein. Moreover, our method allows to follow the uptake of STAT3 loaded vesicles inside cells due to the presence of EGFP in the EGFP-STAT3 fusion protein construct. Taken together, the data presented in this study could provide the scientific background for the development of new therapeutic strategy aimed to restore STAT3 signaling in STAT3 misfunction associated diseases like AD-HIES. In the future, the administration of fully functional wild type STAT3 to CD4+ T cells of AD-HIES patients might compensate its loss of function and would be beneficial for these patients, lowering the risk of infections, the use of medications, and hospitalizations.

Introduction

Extracellular Vesicles (EVs) are a heterogenous group of nano-sized membrane vesicles virtually released by all cell types that transport macromolecules for cell-to-cell communication under physiological and pathological conditions [1–3]. EVs can be isolated from many biological fluids (*e.g.* blood, cerebrospinal fluid, and urine) as well as from conditioned medium of cell culture. Recently, EVs have been proposed as a promising tool for drug delivery because of their natural ability to cross biological barriers, protect their cargo, and selectively target specific cells or tissues [4]. They are not recognized by the immune system as foreign, which reduces the risk of an immune response and

enhances biocompatibility [5–7]. EVs-based drug delivery has shown promise for a variety of applications, including cancer therapy, regenerative medicine, neurodegenerative disease treatment, and immunotherapy. In cancer therapy, EVs have been used to deliver chemotherapeutic agents (*i.e.* paclitaxel [7,8] and doxorubicin [9]) to cancer cells, resulting in reduced tumor growth and improved survival in animal models. Additionally, EVs loaded with small interfering RNAs have been shown to effectively silence target genes in *in vitro* and *in vivo*, demonstrating their potential as gene therapies [10,11]. Moreover, EVs loaded with curcumin, protect mice from lipopolysaccharide-induced brain inflammation with higher effect respect to curcumin alone [12]. Finally, the EVs formulation of catalase has been shown to decrease brain inflammation and increase neuronal survival in a mouse model of Parkinson's disease [13].

Despite the promising results, several challenges still need to be addressed before EVs-based drug delivery can be used in a clinical setting. The major issue is the production of pure EVs with consistent quality and efficacy at large scale. Notably, the lack of standardized methods for EVs isolation and characterization can lead to variability in results and hinder comparability between studies. Nevertheless, the findings on EVs treatment validate them as a useful and promising tool for new therapeutic approaches in different diseases and several clinical trials have recently been reported on the ClinicalTrials.gov database (https://clinicaltrials.gov/).

Autosomal Dominant Hyper-IgE Syndrome (AD-HIES), or Job's syndrome, is a rare primary immunodeficiency and multisystem disorder due to the presence of dominant negative STAT3 mutations [14–18]. Signal Transducer and Activator of Transcription 3 (STAT3) is a latent cytoplasmic transcription factor activated by cytokine and growth factors that transmits signals to the nucleus [19]. In stimulated-cells, STAT3 is recruited to activated receptor tails through its SH2 domains and is phosphorylated at a specific tyrosine residue (TYR^{705}). Tyrosine phosphorylated STAT3 proteins dimerize and the dimer translocates to the nucleus where it promotes the expression of a large variety of genes [20–25]. Under physiological condition the activation of STAT3 is a rapid and transient event that regulates immune response, proliferation, apoptosis, and cell survival [22,23,26]. As described in literature, STAT3 mutations in AD-HIES patient cells hinder the DNA-binding ability of the transcription factor and converge in its loss of function leading to the perturbation of cytokine type and level and to the failure of Th17 CD4$^+$ cell differentiation. These events sensitize patients to recurrent bacterial infection [27,28]. Until now, the discovery of loss of function mutations in *STAT3* gene of AD-HIES patients cells retains only diagnostic value.

Herein, we propose the use of EVs as drug delivery system for the fully functional wild-type STAT3 to restore STAT3 signaling. We set up a simple and versatile method for STAT3 loading in EVs using EGFP-STAT3 fusion protein that provides the opportunity to follow the uptake of loaded vesicles inside cells. Overall, the data of this work represent the essential starting point to develop new therapeutic strategy aimed to restore STAT3 signaling in STAT3 misfunction associated diseases like AD-HIES.

Materials and methods

Chemicals

All chemicals used throughout the present study were of the highest analytical grade, purchased from Sigma-Aldrich (Milwaukee, WI, USA), unless otherwise specified. Roswell Park Memorial Institute (RPMI) 1640 and Dulbecco's Modified Eagle Medium (DMEM) cell culture media, penicillin, streptomycin, gentamycin, sodium pyruvate, phosphate-buffered saline (PBS), Insulin-Transferrin-Selenium-Ethanolamine (ITS-X; Cat. no. 51500056), Fetal Bovine Serum (FBS) were obtained from ThermoFisher Scientific (Waltham, MA, USA). ExpiSf CD medium, enhancer and Expifectamine (Cat. no. A38841), Bac-

to-Bac™ N-His TOPO™ Expression System kit (Cat. no. A11101) containing the pFastBac CT-TOPO vector and the DH10Bac *E. coli* competent cells were purchased from Gibco™ part of ThermoFisher Scientific. Proteinase K (Cat. no. 19131) was bought from Qiagen (Hilden, Germany).

The anti-pTYR^{705} STAT3 (Cat. no. 9131), the anti-rabbit IgG Horseradish Peroxidase (HRP) conjugated secondary antibody (Cat. no. 7074S) and anti-mouse IgG-HRP conjugated secondary (Cat. no. 7076S) antibodies were purchased from Cell Signaling Technology (Danvers MA, USA). The anti-pTYR$^{1007/1008}$JAK2 antibody (Cat. no. 04-1098) was bought from Millipore, (Darmstadt, Germany). The anti-STAT3 (Cat. no. sc-482) and the anti-CD63 (Cat. no. sc-365604) antibodies were obtained from Santa Cruz Biotechnology (Santa Cruz, CA). The Alexa Fluor® 568 anti-rabbit (Cat. no. A11036) was purchased from ThermoFisher Scientific (Waltham, MA, USA).

Protein engineering, expression and purification

A fusion construct comprising 10xHIS N-terminal tagged EGFP, Tobacco Etch Virus (TEV) recognition site and wild-type STAT3 sequence (human isoform, residues 1–770; uniprot ID P40763-1) was generated by overlap extension PCR and cloned into the pFastBac CT-TOPO vector (ThermoFisher Scientific; Cat. no. A11098). The sequence of primers and fusion construct are reported in the Supplementary material. The resulting plasmid was purified, sequence verified and transformed into DH10Bac *E.coli* competent cells. Recombinant bacmid DNA from a positive colony was isolated and used to transfect a suspension culture of ExpiSf9 cells (25 mL, 2.5×10^6 cells/mL) by treatment with Expifectamine according to the manufacturer's instructions. After 96 h the culture medium (P0 viral stock) was isolated by centrifugation and used to generate a new, high titer ($> 10^8$ PFU/mL) P1 baculovirus stock. For protein expression, ExpiSf9 cells were seeded in 30 mL of ExpiSf CD medium at a density of 5×10^6 cell/mL in sterile flasks and grown overnight at 27 °C. The next day, cells were infected with 1 mL of P1 stock (corresponding to a multiplicity of infection (m.o.i.) of ~ 5) and incubated for 72 h at 27 °C with constant shaking at 120 rpm. Cells were harvested and lysed by Dounce homogenization in ice-cold 20 mM Tris HCl pH 7.5, 300 mM NaCl, 20 mM Imidazole, 0.2 % (v/v) NP40, 0.5 mM Tris (2-carboxyethyl) phosphine (TCEP), 5 mM MgCl$_2$ supplemented with 100 Units of DNase (Roche Diagnostics, Rotkreuz, Switzerland), 1 mM PMSF, 1 × SigmaFast™ Protease Inhibitor (Sigma-Aldrich Biotechnology; Cod. no. 11873580001) and 0.1 mM Na$_2$VO$_3$. After centrifugation, the supernatant was loaded onto a 5 mL Nichel chelated agarose resin (Ni^{2+}-NTA; ThermoFisher Scientific; Cat. no. 88221) column equilibrated in 20 mM Tris HCl pH 7.5, 300 mM NaCl, 0.5 mM TCEP supplemented with 20 mM Imidazole. After extensive washing with 20 and 50 mM imidazole, EGFP-STAT3 was eluted with 250 mM imidazole. The purity of the final preparations was checked by SDS-polyacrylamide gel electrophoresis (SDS-PAGE). The green fractions containing EGFP-STAT3 were pooled and concentrated with Amicon® Ultra-15 ultrafiltration device (50 kDa cut-off, Millipore). The protein solution was then loaded on a PD10 desalting column (Cytiva Life Science, Amersham, UK) to completely remove imidazole and exchange the buffer in 20 mM Tris HCl pH 7.5, 150 mM NaCl, 0.5 mM TCEP. All purification steps were carried out at 4 °C.

To obtain wild-type STAT3, the purified EGFP-STAT3 fusion protein was cleaved with TEV protease overnight at 4 °C and further purified by reverse Immobilized Metal Ion Affinity Chromatography (IMAC). As a final step of purification, STAT3 was fractionated by Size Exclusion Chromatography (SEC) using a SuperdexG200 column equilibrated with 20 mM Tris HCl pH 7.5, 150 mM NaCl. The chromatographic run was performed using a 0.4 mL/min flow rate with detection at 280 nm in an ÄKTA prime plus system (Pharmacia, Uppsala, Sweden) and fractions of 0.5 mL were collected with an automatic sampler collector.

Circular dichroism

Far and near UV Circular Dichroic (CD) spectra were registered on Jasco J-715 spectropolarimeter equipped with a Peltier system to keep the sample compartment at 25 °C. Far UV spectra were registered in 1 mm quartz cuvette with 1–1.5 μM recombinant proteins in buffer 20 mM Tris HCl pH 7.5, 150 mM NaCl, 0.5 mM TCEP. Near UV spectra were recorded using a 10 mm quartz cuvette with 3.5–4 μM recombinant proteins in buffer 20 mM Tris HCl pH 7.5, 150 mM NaCl, 0.5 mM TCEP. Routinely, three spectra for Far- UV and five for Near UV were recorded at a scan speed of 50 nm min^{-1} with a bandwidth of 1 nm. Thermal denaturation of EGFP-STAT3 (1 μM) and STAT3 (3.3 μM) was monitored between 15 °C and 90 °C using the same conditions as for the far-UV spectra. The ellipticity signal at 208 nm (θ_{208}) was recorded at a scan rate of 1.5 °C/min and at a response time of 4 s, using a 0.1 cm quartz cuvette. Mean residue ellipticity $[\theta]_{MRW}$ (deg cm^2 dmol^{-1}) was calculated according to the formula:

$$[\theta]_{MRW} = (\theta/10)(MRW/lc)$$

where θ is the registered ellipticity (in mdeg), MRW is the mean residue weight of the protein, l is the pathlength (in cm) and c is protein concentration (in mg/mL). Secondary structure estimation has been performed using BeStSel online tool [29].

STAT3/JAK2 in in vitro kinase assay

STAT3/JAK2 kinase assay was performed using recombinant JAK2 active protein (Sigma-Aldrich Biotechnology Cat. no. 14-640), as previously described [30]. Briefly, kinase reactions were performed by incubating 500 ng of EGFP-STAT3 or STAT3 with 50 ng of recombinant JAK2 active protein in 15 μL of kinase reaction buffer (20 mM Tris HCl pH 7.5, 50 mM MgCl$_2$, 100 μM ATP) within the linear reaction range. The reaction mixtures were incubated for 30 min at RT under mild agitation. The reactions were quenched by the addition of reducing Laemmli Sample Buffer followed by heating at 95 °C for 5 min. The samples were then separated by 7.5 % SDS-PAGE, transferred on a PVDF membrane (Immobilon P, Millipore) and probed with anti-pTYR^{705} STAT3 antibody. After washings with Tris-buffered saline plus 0.1 % (v/v) Tween 20 (TBST), the membrane was hybridized with anti-rabbit IgG-HRP conjugated secondary antibody and developed by Western Chemiluminescent HRP Substrate (Millipore, Cat. No. WBKLS0500) using ChemiDoc XRS Imaging System (Bio-Rad, Feldkirchen, Germany). Blotted proteins were quantified using ImageLab (Bio-Rad).

To verify the autophosphorylation of JAK2, membranes were re-hybridized with anti-pTYR$^{1007/1008}$JAK2 antibody and recognized with anti-rabbit IgG-HRP secondary antibody. After stripping, membranes were re-hybridized with rabbit anti-STAT3 antibody.

Cells culture

Human B lymphoblastoid cells RO (DSMZ-German Collection of Microorganisms and Cell Cultures GmbH, Braunschweig, Germany, ACC 452) were cultured in 5 % CO$_2$ incubator at 37 °C using RPMI 1640 cell culture medium supplemented with 10 % (v/v) FBS, 100 IU/mL penicillin and 100 μg/mL streptomycin (Medium A). The cells were sub-cultured every 3–4 days. Before EVs isolation, the FBS was gradually replaced with RPMI 1640 medium supplemented with 1 % (v/v) ITS-X and 1 mM Sodium Pyruvate (Medium B). Specifically, the percentage of Medium A were lowered to 50 %, 25 % and 0 % using Medium B at each sub-culturing step. Then, cells were seeded at 0.35×10^5 cells/mL and after 48 h the cells conditioned culture media were collected. The collected media were stored at − 80 °C, up to 2 months.

Human breast cancer cell line MDA-MB231 (American Type Culture Collection, ATCC Manassas, VA) was cultured in DMEM supplemented with 10 % FBS, 100 IU/mL penicillin, 50 μg/mL streptomycin, and 40 μg/mL gentamycin in a 5 % CO$_2$ atmosphere at 37 °C.

Peripheral blood mononuclear cell (PBMC) samples from healthy donors were collected at the Hematology Unit of Verona, upon approval by the local Ethics Committee. In accordance with the Declaration of Helsinki, all subjects provided written informed consent to the use of their biological material for research purposes. Cells were grown in RPMI-1640 plus 10 % FBS, 50 U/mL penicillin and 50 μg/mL streptomycin under 5 % CO$_2$ humidified air at 37 °C.

EVs isolation and purification

Isolation and purification of EVs were performed as previously described [31], with some modifications. Firstly, 400 mL of RO cells (2×10^8 cells) conditioned medium was centrifuged sequentially at $300 \times g$, $2000 \times g$ and $9500 \times g$ to remove dead cells and debris. After two filtration steps with 0.45 μm and 0.22 μm sterile syringe filters, the medium was ultracentrifuged at $100,000 \times g$ for 2 h at 4 °C (Rotor SW 45 Ti, Optima XPN-80 Ultracentrifuge Beckman Coulter, Lifesciences) and the obtained pellet was resuspended in 500 μL PBS. EVs were purified by SEC on Sepharose CL-2B column (Cytiva Life Science), collecting 1 mL fractions with PBS as elution buffer. The collected fractions were analyzed for protein content and particle size distribution as described below. The EVs-enriched SEC-fractions were pooled and concentrated by further ultracentrifugation step at $100,000 \times g$ for 2 h at 4 °C (Rotor SW 45 Ti, Optima XPN-80 Ultracentrifuge Beckman Coulter, Lifesciences).

Encapsulation of EGFP-STAT3 in EVs

EGFP-STAT3 was loaded into isolated EVs using a saponin-assisted encapsulation method [32]. For protein loading, EVs suspension (10^{11}–10^{12} particles/mL) was incubated with 2 to 0.1 mg/mL EGFP-STAT3 recombinant protein and 0.4 mg/mL saponin for 30 min at 25 °C. Then, loaded EVs were purified by SEC using Sepharose CL-2B as described above. Isolated loaded EVs were directly used or stored at − 20 °C until further analysis.

Characterization of EVs

The particle concentration and size distribution were determined by Nanoparticle Tracking Analysis (NTA) using NanoSight NS300 (Malvern Instruments, UK). Samples were diluted up to $1000 \times$ in PBS in order to have a concentration of 10–100 particles per frame. For each sample, three videos of 60 s each were recorded, and the camera level was set to give a clear sharp image of the particles. The acquired videos were analyzed using NanoSight 2.3 software with a detection threshold from 3 to 5 and only the measurement within the linear range of the instrument have been considered.

Surface charge on the EVs was determined in terms of Zeta Potential by Dynamic light scattering (DLS) using Zetasizer Nano-S (Malvern Instruments, UK).

For Transmission electron microscopy (TEM) analysis, 5 μL of the EVs sample was applied onto on an ultra-thin carbon coated copper grid (CF200H-Cu-UL, Electron Microscopy Sciences) and incubated for 10 min at 37 °C. Images were acquired using a TEM Morgagni 268D (FEI Philips, Oregon, United States) at 80 kV.

Protein concentration assessment

Protein concentration of each sample was measured by Bicinchoninic acid (BCA) assay kit following the manufacturer's instructions (ThermoFisher Scientific; Cat. no. 23227). Before each measurement, Bovine Serum Albumin (BSA) calibration curve was prepared in triplicate. The measurements were performed with a Multiplex M Nano microplate reader (Tecan, Männedorf Switzerland).

EGFP-STAT3 quantification

EGFP-STAT3 was quantified by measuring the fluorescence emission of EGFP at 535 nm upon excitation at 485 nm. A six-point calibration curve (100, 50, 15, 12.5, 6.25, 0 μg/mL) was prepared in triplicate starting from EGFP-STAT3 recombinant protein at known concentration. The fluorescence measurements were performed using black 96-wells plate with a Multiplex M Nano microplate reader (Tecan, Männedorf Switzerland).

Protein slot blot

The assay was performed using a Bio-Dot® SF Microfiltration Apparatus (Bio-Rad, Feldkirchen, Germany) following the manufacturer's instructions. The indicated volume of samples was loaded on each well and blotted onto nitrocellulose membrane (Bio-Rad, Feldkirchen, Germany). The membranes were incubated with anti-CD63 and anti-STAT3 antibodies. After washing with TBST, the membranes were hybridized with anti-mouse IgG-HRP conjugated secondary antibody and developed by Western Chemiluminescent HRP Substrate (Millipore, Darmstadt, Germany) using ChemiDoc XRS Imaging System (Bio-Rad, Feldkirchen, Germany). Blotted proteins were quantified using Image-Lab (Bio-Rad).

Proteolytic digestion of EGFP-STAT3 loaded EVs-proteinase K assay

To set up the proteinase K digestion, equal amount of purified EGFP-STAT3 were digested 0.5 to 3 h at 37 °C using protease:protein ratio 1:100 (w/w). The reactions were stopped by the addition of reducing Laemmli sample buffer and the proteolysis mixtures were resolved by SDS-PAGE using two 10% polyacrylamide gel. The first gel was stained with Coomassie Brilliante blue (Fig. S1 A) and the second one was analyzed by Western Blot using anti-STAT3 antibody (Fig. S1 B). Specifically, after SDS-PAGE the separated proteins were transferred to the PVDF membrane, probed with anti-STAT3 antibody and recognized with anti-rabbit IgG peroxidase-conjugated secondary antibody. Finally, the membrane was developed by Western Chemiluminescent HRP Substrate (Millipore) using ChemiDoc XRS Imaging System (Bio-Rad). Blotted proteins were quantified using ImageLab (Bio-Rad).

To assess EGFP-STAT3 encapsulation, equal protein amount of EGFP-STAT3 loaded EVs were lysed with 2 % SDS solution for 30 min at 25 °C and then treated or not with proteinase K for 1 h at 37 °C. The same amount of loaded EVs was treated with protease without any lysis treatment. Control loaded EVs underwent the same procedure without any protease or SDS lysis treatment. The proteolysis mixture was resolved on 10 % SDS-PAGE and analyzed by Western Blot using anti-STAT3 antibody as previously described. The proteolytic digestion of loaded EVs is shown in the schematic workflow (Fig. S2).

EVs cellular-uptake

For cellular treatment, loaded and unloaded EVs were stained with DiD, a lipophilic carbocyanine membrane dye (Molecular Probes Inc., Cat. no. V22889) and purified by SEC as described above.

MDA-MB231 cells and freshly prepared PBMCs, were seeded into 24-wells plate at density 0.9×10^5 and 1×10^5 cells/well, respectively. After 2 h the cells were treated with loaded or unloaded EVs in fresh medium for 24 h. Then, the cells were washed two times with PBS and cyto-centrifuged at 500 x g for 5 min on glass slides. Air-dried cytospins were fixed with 4 % (v/v) paraformaldehyde for 1 h at RT. Fixed cells were permeabilized with 0.1 % (v/v) Triton X-100 in PBS for 5 min and blocked with 5% (w/v) BSA + 0.05 % (v/v) Triton X-100 in PBS for 1 h at RT under agitation. Then, samples were incubated with anti-pTYR[705] STAT3 antibody overnight at 4 °C. After incubation, cells were washed three times for 3 min with PBS, incubated with Alexa Fluor® 568 anti-rabbit (ThermoFisher Scientific for 1 h at RT, and counterstained with

4′,6-diamidino-2-phenylindole (DAPI, ThermoFisher Scientific) for 15 min at RT. Cell images were captured using a confocal laser-scanning fluorescence microscope Leica SP5 (Leica Microsystem, Wetzlar Germany) at 63 × magnification and processed using Adobe Photoshop and ImageJ software. The nuclear localization of phosphorylated STAT3 was analyzed by ImageJ software by orthogonal view tool.

Results

Expression, purification, and biophysical/biochemical characterization of EGFP-STAT3

To produce sufficient amount of full length recombinant STAT3 protein, load it in EVs, and follow its cellular uptake, EGFP-STAT3 fusion protein was expressed in Sf9 cells and purified by Ni^{2+} affinity chromatography to homogeneity at an apparent molecular weight of around 120 kDa (Fig. S3 A and B). The CD spectrum of the fusion protein in the Far-UV region shows the typical dichroic signal of a protein rich in α-helix secondary structure (Fig. 1A, red line). The CD spectrum of wild-type recombinant STAT3, purified as described in the Supplementary Section (Fig. S4 A–C), is shown for comparison (Fig. 1A, black line). The estimated secondary structure content is different from that of STAT3 [33,34] with a drop in the α-helix content and an increase in β- and random coil structures (Table 1). These differences can be ascribed to the presence of the EGFP domain, which is mainly composed of β-strands [35]. In the near-UV region, EGFP-STAT3 displays a predominant contribution of EGFP protein at 260–290 nm (Fig. 1B, red line) when compared to the near-UV spectrum of STAT3 (Fig. 1B, black line). Moreover, the thermal stability of EGFP-STAT3 protein was investigated by monitoring the ellipticity at 208 nm between 10 and 96 °C. EGFP-STAT3 exhibits a sigmoidal trend compatible with a two-state unfolding process and melting temperature (T_m) compatible with that of wild-type STAT3 (EGFP-STAT3 $T_m = 55$ °C; STAT3 $T_m = 55.34$ °C) (Fig. 1C).

As described in literature, one of the critical steps in the activation of STAT3 signaling is its phosphorylation at tyrosine 705 residue, dimerization and successive translocation into the nucleus [25,26]. As shown in Fig. 2, EGFP-STAT3 was successfully phosphorylated by JAK2 active kinase, providing evidence of the proper accessibility of the TYR[705] residue. Notably, the anti-pTYR[705] STAT3 antibody recognized the fusion protein in absence of kinase indicating that the recombinant protein is already partially tyrosine phosphorylated (Fig. 2).

Taken together, these data suggest a proper folding of EGFP-STAT3 protein.

Encapsulation of EGFP-STAT3 into EVs and their characterization

EVs were isolated from human B-lymphoblastoid RO cells, a commercially available cell line obtained from a patient with severe combined immunodeficiency. These cells do not express MHC class II complexes and are characterized by low immunogenicity [36].

EVs were isolated from RO cells conditioned serum-free culture medium by ultracentrifugation, purified by SEC and characterized (Fig. S5 and S6). The isolation and characterization results are in line with those previously obtained with the same methodologies strengthening the effectiveness of the used protocols [31,37].

The EGFP-STAT3 fusion protein was loaded into EVs by saponin-assisted drug loading approach [32]. Briefly, after incubation of the ultracentrifuged EVs pellet with EGFP-STAT3, loaded EVs were purified by SEC to remove free fusion protein and undesired components. The SEC profile presents two main total protein peaks at the same elution volume of unloaded EVs (Fig. 3A). The fluorescence emission signal, corresponding to EGFP-STAT3, was revealed in the enriched EVs fractions, suggesting successful loading of the fusion protein into EVs (Fig. 3B). The size of the loaded particles is in the range of EVs and confirms the recovery of EVs (Fig. 4A). As for unloaded EVs, each
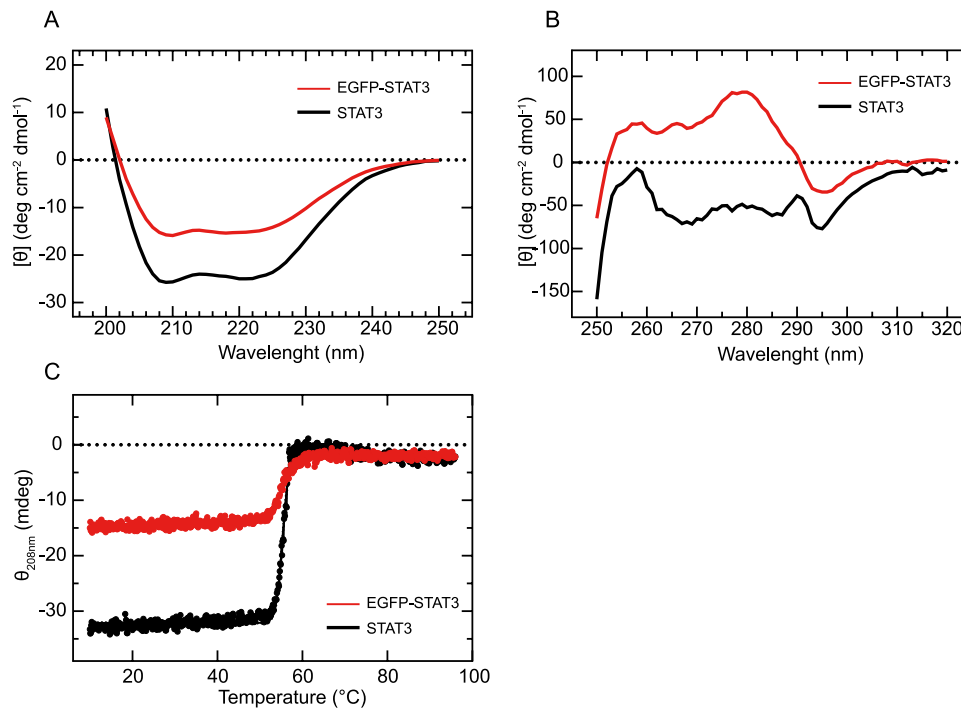
Fig. 1. Biophysical characterization of EGFP-STAT3 fusion protein. (A) CD spectra in Far-UV. (B) CD spectra in Near-UV. (C) Thermal denaturation. EGFP-STAT3, red line; STAT3, black line.

Table 1
Secondary structure content of STAT3s protein. Values are expressed in percentages. [a] Values reported from [26].

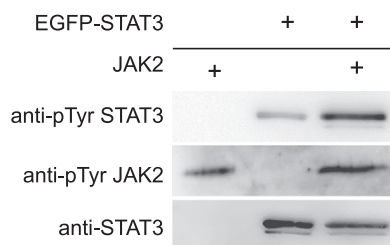|	α-Helix	β-structure	Random coil
STAT3 (124-732)[a]	67.4	14.9	17.7
STAT3	67.3	8.9	23.8
EGFP-STAT3	37.7	17	45.3

Fig. 2. In *in vitro* JAK2 kinase assay. In *in vitro* JAK2 kinase assay was performed using JAK2 active protein and EGFP-STAT3 recombinant protein. Western Blot analysis shows that JAK2 increases EGFP-STAT3 TYR^{705} phosphorylation, a pre-requisite for STAT3 functionality (lane 3). The kinase assay was also performed using EGFP-STAT3 purified protein without JAK2 kinase confirming its intrinsic phosphorylation (lane 2). Moreover, as negative control, EGFP-STAT3 was omitted in lane 1. The images are representative of 4 independent experiments.

fraction was then analyzed by Slot Blot using anti-CD63 antibody. The data confirm the nature of isolated particles (Fig. 4B).

The EVs-enriched fractions were collected, pooled and analyzed by TEM. The images confirmed the overall cup-shaped and spherical shape of the EVs with a visible lipid bilayer. Moreover, the size range (80–150 nm) and mean diameter of the EVs (~ 120 nm) matched the NTA data (Fig. 5).

The EVs-enriched fractions were then analyzed by NTA in scattering and fluorescence modes. It should be noted that scattering analysis considers all the particles present in the sample, whereas fluorescence reveals only EGFP-STAT3-loaded particles. The NTA analysis showed that total particles number in the scattered mode was higher than that in fluorescence mode (Fig. 6A and B, white bar).

Finally, DLS measurements indicated a low zeta potential at − 18.30 ± 0.94 mV and confirmed the average diameters measured by NTA and TEM. Notably, saponin treatment did not alter zeta potential of loaded EVs respect to unloaded EVs (− 18.90 ± 0.76 mV). The negative surface charge is important for the stability of EVs in suspension and their uptake by cell membrane [38]. These data are in line with those reported in literature [31,37].

Then, the pooled fractions were concentrated by a second ultracentrifugation step and analyzed by NTA. The scattering mode measurements revealed that the recovery of EVs after ultracentrifugation was around 15 % (Fig. 6A, grey bar). On the other hand, the analysis of the same sample in fluorescent mode showed that all the fluorescent EVs were recovered after ultracentrifugation (Fig. 6B, grey bar). Intriguingly, these data suggest an enrichment of the fluorescent positive fraction during the second ultracentrifugation step.

To confirm and quantify EGFP-STAT3 loaded in EVs, different concentrations of EGFP-STAT3 recombinant protein, the pooled and pooled/concentrated fractions were loaded on the gel and analyzed by Slot Blot using an anti-STAT3 antibody (Fig. 7A). The chemiluminescent bands on the membrane were quantified by densitometric analysis (Fig. 7B). The protein calibration curve was build using the membrane densitometric data (Fig. 7C). The densitometric analysis of the bands indicates that 2.7 ± 0.9 μg and 2.5 ± 1.0 μg of EGFP-STAT3 were associated with the pooled EVs and pooled/concentered EVs, respectively. These data further confirm the recovery of STAT3 fusion protein associated with EVs after ultracentrifugation step.

To assess if EGFP-STAT3 is localized in the EVs lumen, proteinase K assay on the pooled and concentrated fractions was performed. If the cargo protein is localized inside the nanoparticles, it should be protected from the protease that is not able to penetrate through the lipidic bilayer. Conversely, if the cargo protein adheres outside the membrane, it is exposed to protease activity and is sensitive to digestion. On the basis of the results obtained by the digestion of EGFP-STAT3 (Fig. S1),
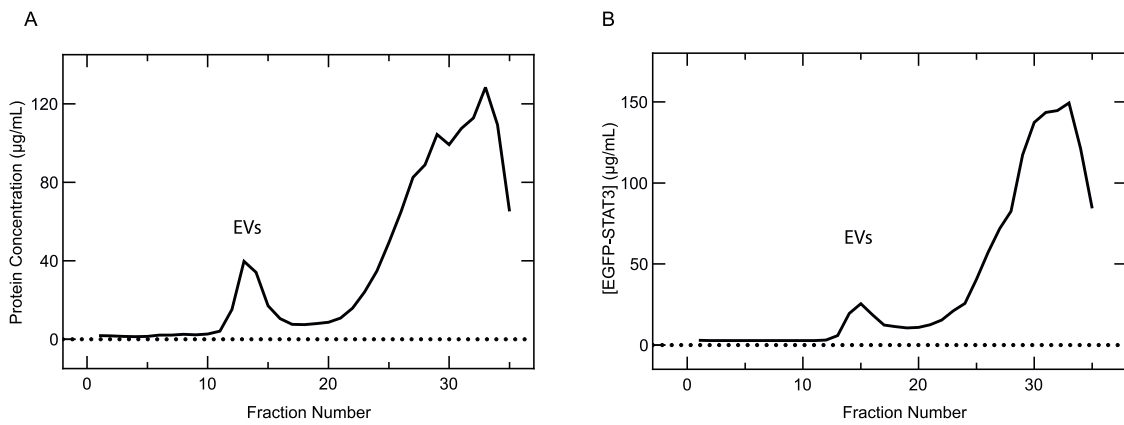
Fig. 3. SEC chromatographic profiles of EGFP-STAT3 loaded EVs. EGFP-STAT3 loaded EVs were purified by SEC. The total protein content and EGFP-STAT3 concentration were analyzed in each collected fraction as described in Material and Method Section. (A) The SEC elution profile built using total protein concentration measured by BCA assay. (B) The SEC elution profile built using EGFP-STAT3 concentration measured by fluorescence method (λ_{ex}535 nm/λ_{ex} 485 nm). The images are representative of 10 independent experiments.
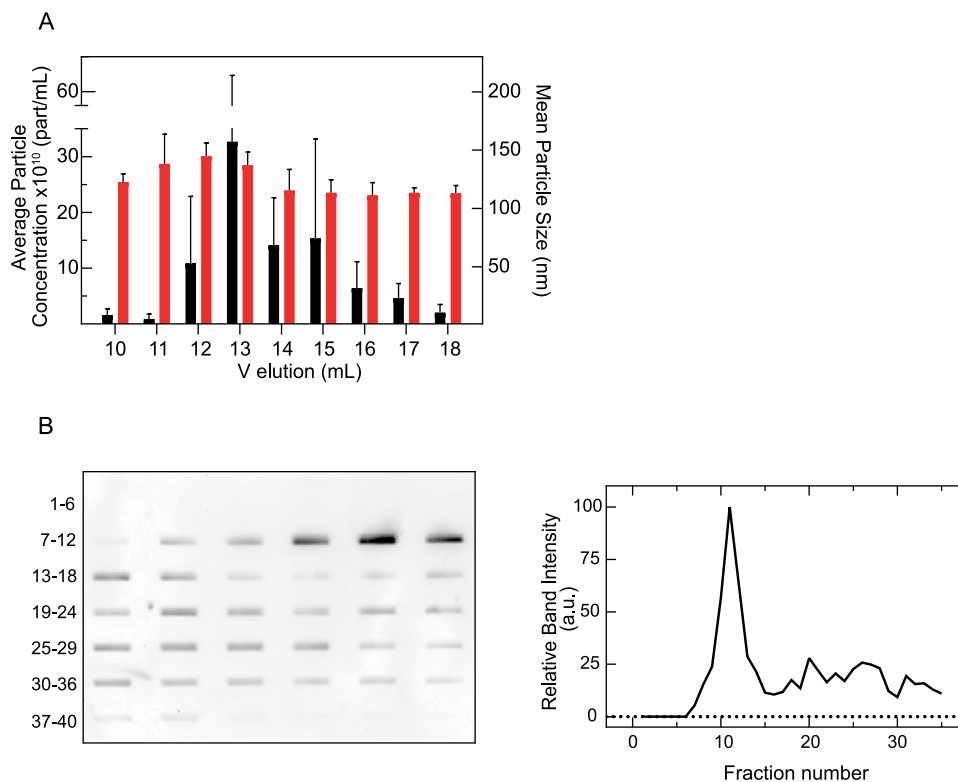

Fig. 4. Characterization of the SEC EVs-enriched fractions. EGFP-STAT3 loaded EVs were purified by SEC and 1 mL fractions were collected. (A) Graph represents average particle concentration (black bars) and mean particle size (red bars) for the EVs-enriched SEC fractions (n = 5 biological replicates, mean ± SD). (B) Slot Blot of SEC eluted fractions probed with anti-CD63 antibody. (C) Chromatographic profile of SEC obtained by the densitometric analysis of bands membrane. The images are representative of 5 independent experiments.

the proteinase K assay of loaded EVs was carried out for 1 h at 37 °C. As shown in Fig. 8, the proteolytic digestion is more extended when the EVs have been lysed by SDS and then subjected to protease treatment in comparison to the other treatment conditions.

Evaluation of EGFP-STAT3 EVs uptake by cells

For the setting up of the EVs uptake experiment, MDA-MB231 cells were treated with EVs and observed at different time points with a fluorescent microscope (Zeiss Axio Imager) to survey the possible interaction between the EVs and the cells (data not shown). On the basis

of these data, 0.9×10^5 MDA-MB231 cells were treated with around 1.5×10^{10} EGFP-STAT3 loaded EVs for 24 h and analyzed by confocal microscopy to evaluate their uptake (Fig. 9). Confocal microscopy images allow not only to verify the presence of EGFP-STAT3 inside the cells but also investigate the phosphorylation of the transcription factor thanks to the use of the anti-pTyr705-STAT3 antibody. The recombinant fusion protein is highlighted by fluorescence emission of EGFP tag (green), EVs by fluorescence emission of DID (magenta) and nuclei by fluorescence emission of DAPI (cyan). It is important to note that the anti-pTyr[705]-STAT3 antibody (red) recognized only the exogenous STAT3 since the endogenous transcription factor is not phosphorylated
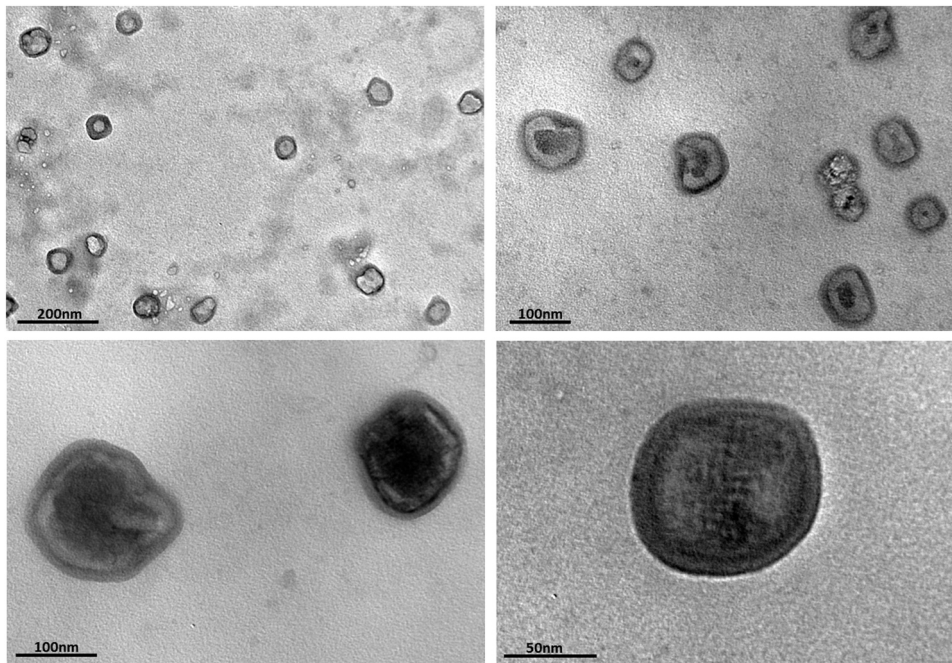
Fig. 5. TEM analysis of pooled EVs fractions. TEM analysis of EGFP-STAT3 loaded EVs purified by ultracentrifugation and SEC. Representative images at the indicated scale bars. Magnification: up/left 44,000 ×, up/right 56,000; down/left: 71,000 ×; down/right 140,000 ×.
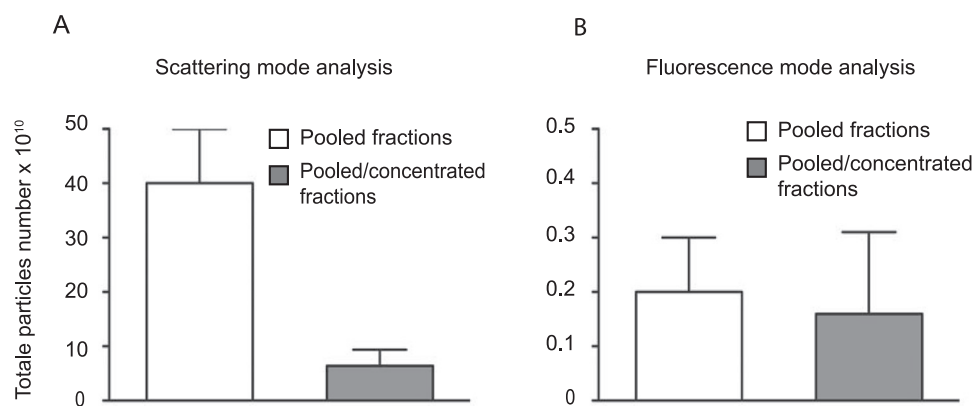

Fig. 6. NTA of pooled EGFP-STAT3 EVs fractions. The pooled EGFP-STAT3 EVs fractions (white bars) and pooled/concentrated EGFP-STAT3 EVs fractions (grey bars) were analyzed by NTA. (A) NTA scattering mode; pooled/pooled and concentrated ratio is 6.4. (B) NTA fluorescence mode; pooled/pooled and concentrated ratio is 1.25. Bars represent total average particles number of 4 independent experiments (mean ± SD).

without appropriate stimuli in MDA-MB231 cell line. The presence of co-localization of red and green signals in the merge images (yellow) demonstrates that the internalized protein is tyrosine phosphorylated, a prerequisite to the functional activity of the transcription factor. These signals are near the nucleus (cyan) of cells highlighting STAT3 cyto-plasm /nucleus trafficking (Fig. 9).

To investigated if EVs are reliable delivery system of wild type STAT3 to blood cells, 1×10^5 PBMCs were seeded in 24 wells plate, treated with 5×10^{10} EGFP-STAT3 EVs and analyzed by confocal microscopy. As shown in Fig. 10**B**, STAT3 positive cells (green) were detected in PBMCs treated with EGFP-STAT3 loaded EVs. The internalized EGFP-STAT3 is tyrosine phosphorylated as revealed by anti-pTYR[705] STAT3 antibody staining (red). The presence of co-localization of red and green signals in the merge images highlighted in yellow, demonstrate that internalized protein in phosphorylated at tyrosine 705 residue. The Z-stack analysis revealed that phosphorylated EGFP-STAT3 translocated into the nuclei, confirming the physiological trafficking of the tran-scription factor (Fig. 10**C**). Unloaded EVs were used as control

(Fig. 10**A**).

Discussion

Over the last decade, EVs-based drug delivery systems have attracted considerable interest as they may offer unique and new properties for drug delivery [39]. Their natural origin, protein and nucleic acid composition, and intrinsic pleiotropic therapeutic effects could enable new possibilities in the field of drug delivery and potentially succeed where conventional drug delivery systems fail. Importantly, EVs exhibit low immunogenicity and ability to escape the immune clearance although these hypotheses need to be investigated for each formulation. Moreover, EVs can cross tissue, cellular and intracellular barriers, including the blood brain barrier through transcytotic processes or small vessel opening, or by exploiting the enhanced permeability and reten-tion effect [40,41].

In the last years, proteins and peptides treatment have been proposed as pharmacological approaches in protein replacement therapy and
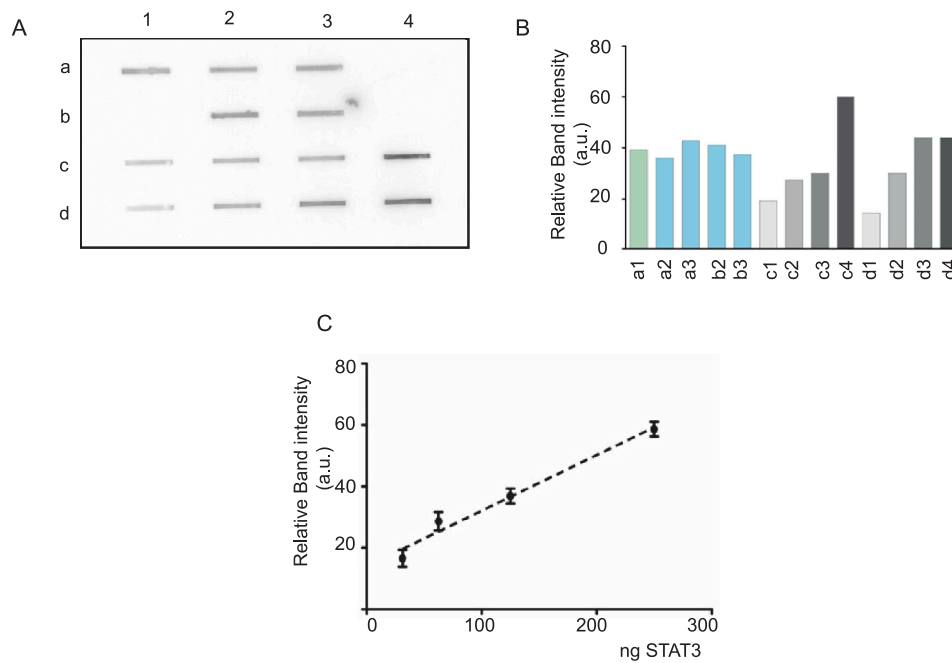
Fig. 7. Quantification of EGFP-STAT3 loaded into EVs. (A) Slot Blot of EGFP-STAT3 recombinant protein, pooled EGFP-STAT3 EVs and pooled/concentrated EGFP-STAT3 EVs probed with anti-STAT3 antibody. a1: pooled EGFP-STAT3 EVs; a2, a3, b2 and b3: equal amount of pooled/concentrated EGFP-STAT3 EVs; c1 and d1: 32.25 ng of EGFP-STAT3 recombinant protein; c2 and d2 of 62.5 ng EGFP-STAT3 recombinant protein; c3 and d3 125 ng of EGFP-STAT3 recombinant protein; c4 and d4 125 ng of EGFP-STAT3 recombinant protein. (B) Densitometric analysis of membrane. Green: pooled EGFP-STAT3 EVs; Light blue: pooled/concentrated EGFP-STAT3 EVs; Grey scale: EGFP-STAT3 calibration curve. (C) Calibration curve of EGFP-STAT3 recombinant protein plotted with the densitometric analysis data of 5 independent calibration curves. The image is representative of 5 independent experiments.
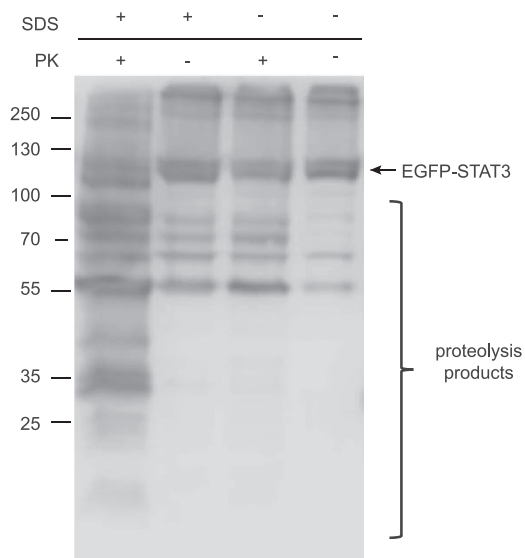

Fig. 8. Proteinase K assay. Western Blot analysis of loaded EVs subjected to proteinase K assay. EGFP-STAT3 loaded EVs and with or without proteinase K were incubated at 37 °C for 1 h. The anti-STAT3 antibody was used to detect the transferred protein. The image is representative of 4 independent experiments.

protein misfolding treatment [42–46]. However, stability, aggregation tendency, short elimination half-life, and immunogenicity of proteins have limited their clinical use [47]. To overcome these challenges, various synthetic nanoparticles and, recently EVs, have been proposed for protein delivery.

In this work, we developed a novel EVs-based system able to deliver STAT3 protein inside cell nucleus. This set the first step for the development of delivery system able to restore STAT3 signaling as a possible therapeutic strategy in STAT3 misfunction associated diseases.

Firstly, EGFP-STAT3 fusion protein was designed to introduce a tracking moiety for STAT3 in the EVs formulation and in *in vitro* cell experiments. Notably, the baculovirus expression system offers the advantage of producing proteins bearing appropriate post-translational modifications. These proteins are antigenically, immunogenically, and functionally more similar to the native human protein than those expressed in yeast or other eukaryotes [48]. Our data revealed that the insect cells produce a properly folded and partially tyrosine phosphorylated EGFP-STAT3. To the best of our knowledge, this is the first report on the production of this fusion protein that could be a useful tool in the research field of STAT3 trafficking.

Then, we set up a protocol for the encapsulation of the EGFP-STAT3 protein in EVs purified from RO cells culture media. These cells, isolated from a severe combined immunodeficiency patient, lack MHC class II molecules and have a potentially favorable biocompatibility [36].

As previously described, ultracentrifugation technique, combined with SEC purification, allows to obtained purified EVs with chemical-physical characteristics in line with the Minimal Information for Studies of Extracellular Vesicles (MISEV) guidelines [49]. Indeed, the isolated EVs presented a size distribution in the range of 100–150 nm, a cup morphology with lipid bilayer and typical surface marker as CD63. EGFP-STAT3 fusion protein was encapsulated post-EVs-isolation by permeabilization with saponin, a mild loading agent that did not induce significant changes in EVs membrane morphology and in EVs average size and zeta potential. Several methods have been developed for post-EVs-isolation loading, including sonication, electroporation and freeze-thaw cycles. Although sonication and extrusion result in major loading efficacy, they can permanently damage EVs membrane and cause aggregation of therapeutic agent [13,32,50]. Specifically, since STAT3 is a protein characterized by the presence of exposed hydrophobic patches and, on the basis of our experience, by an high aggregation tendency we chose to avoid these methods. As suggested by the analysis of confocal microscopy images, the use of saponin assisted method preserve the folding state and functional activity of STAT3.
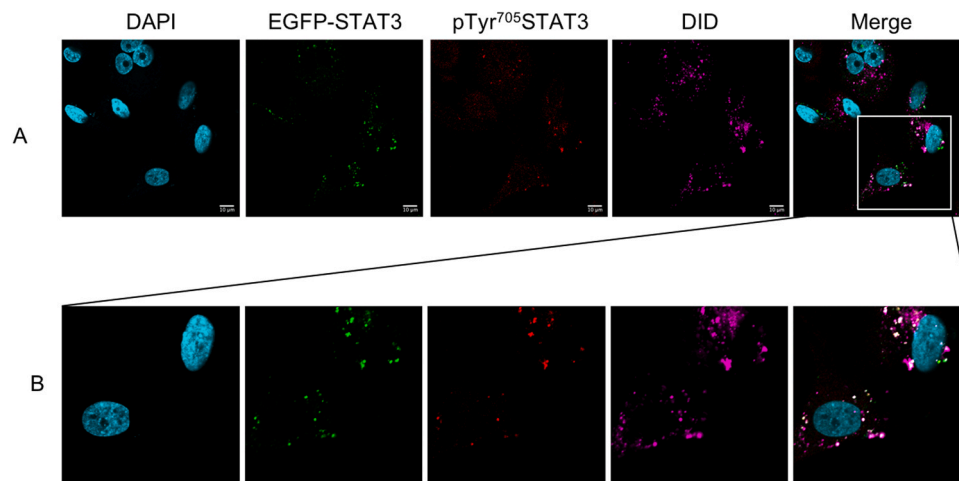
Fig. 9. Confocal microscopy of MDA-MB231 cells treated with EGFP-STAT3 EVs. The cells were treated with unloaded and loaded EVs for 24 h and images were acquired by a confocal laser-scanning microscope using a 63 × objective lens. EGFP-STAT3 positive cells (green), pTYR[705] STAT3 positive cells (red); DID-EVs (magenta); DAPI-nuclei (cyan). Scale bar 10 μm. The presence of co-localization of red and green signals in the merge images was highlighted in yellow. (A) Representations of MDA-MB231 after treatment with loaded EVs. (B) Zoom of merge. Images are representative of 3 different experiments.

Fluorescence measurement and Slot-Blot analyses with anti-STAT3 antibody demonstrated that only a part of recombinant fusion protein was encapsulated into EVs but the obtained formulation successfully delivers STAT3 protein into PBMCs nucleus as revealed by confocal microscopy images. As expected, STAT3 enters the nucleus of cells due to the presence of phosphorylation at its TYR[705] residue, a prerequisite to the functional activity of the transcription factor. It is important to note that only a small number of papers described the encapsulation of protein into EVs and only part of them reports a post-EVs isolation approach to achieve the protein loading [13,32,50,51].

Once established the association of STAT3 with the isolated EVs we questioned whether EGFP-STAT3 was mainly located inside the lumen of the EVs or merely interacting with the external portion of the membrane lipidic bilayer. The need to determine the topology of EVs-associated components has been widely discussed by the EVs scientific community [49,52] Recently, Rankin-Turner et al. underlined the importance of being able to distinguish whether the therapeutic cargo is luminally incorporated or only associated with EVs [53]. This would be of utmost importance for the correct determination of encapsulation efficiency and loading capacity, and therefore, for the definition of the most effective criteria for EVs drug loading. The results of the proteinase K assay, proposed in this paper, point out that the main portion of the EVs-associated EGFP-STAT3 is protected by the EVs membrane and is not sensitive to digestion, suggesting the successful incorporation of EGFP-STAT3 inside EVs.

Regarding the delivery of STAT3, this study demonstrated the ability of EVs to interact with target cells, cross blood cells membrane and release STAT3 in the cell cytoplasm. This aspect might be crucial for treatment of STAT3 misfunction related diseases.

Conclusion

Overall, the data of this work represent the essential starting point to develop a new therapeutic strategy aimed to restore STAT3 signaling in STAT3 misfunction related diseases, like AD-HIES. Despite the central role of STAT3 in the pathogenesis of this disorder, no therapeutic approach is nowadays available to restore STAT3 signaling. The administration of fully functional wild type STAT3 to CD4+ T cells from AD-HIES patients might compensate STAT3 loss of function and enhance the differentiation into T_H17 cells. In a future personalized therapy, the use of EVs isolated in autologous manner for re-administration to the patient after loading of the therapeutic cargo might be a promising alternative approach to conventional therapy. Preclinical and clinical trials support the use of autologous EVs obtained by peripheral-blood or derived by cultured primary monocytes, indicating that autologous EVs administration is safe and well tolerated. However, further efforts are needed to standardize the EVs isolation procedure and the drug loading, thereby generating more consistent, clinically applicable, therapeutic products.

Ethics approval and consent to participate

blood samples from healthy donors were collected at the Hematology Unit of Verona, upon approval by the local Ethics Committee. In accordance with the Declaration of Helsinki, all subjects provided written informed consent for the anonymous collection and use of their biological material for research purposes.

CRediT authorship contribution statement

EB and SM conceptualized the work. IB and AKE performed experiments for protein production and characterization. IB, MB, M.A.T PB and EB conducted the experiment for preparation, characterization and loading of EVs. MB, EB and IF performed cells experiments. SC supervised the protein production experiment. GF supervised the EVs preparation experiments. SM and EB coordinated and supervised all the work, helped with data analysis and interpretation, and wrote the first draft of the manuscript. The manuscript was written through contributions of all authors. All authors have given approval to the final version of the manuscript.

CRediT authorship contribution statement

Gregor Fuhrmann: Supervision, Funding acquisition. **Sofia Mariotto:** Writing – review & editing, Writing – original draft, Validation, Supervision, Funding acquisition, Conceptualization. **Ilaria Bettin:** Methodology, Investigation, Data curation. **Martina Brattini:** Methodology, Investigation. **elena Butturini:** Writing – review & editing, Validation, Supervision, Methodology, Investigation, Conceptualization. **Muhammed Ashiq Thalappil:** Investigation. **Paolo Bernardi:** Investigation. **Elham Ataie Kachoie:** Investigation. **Stefano Capaldi:**
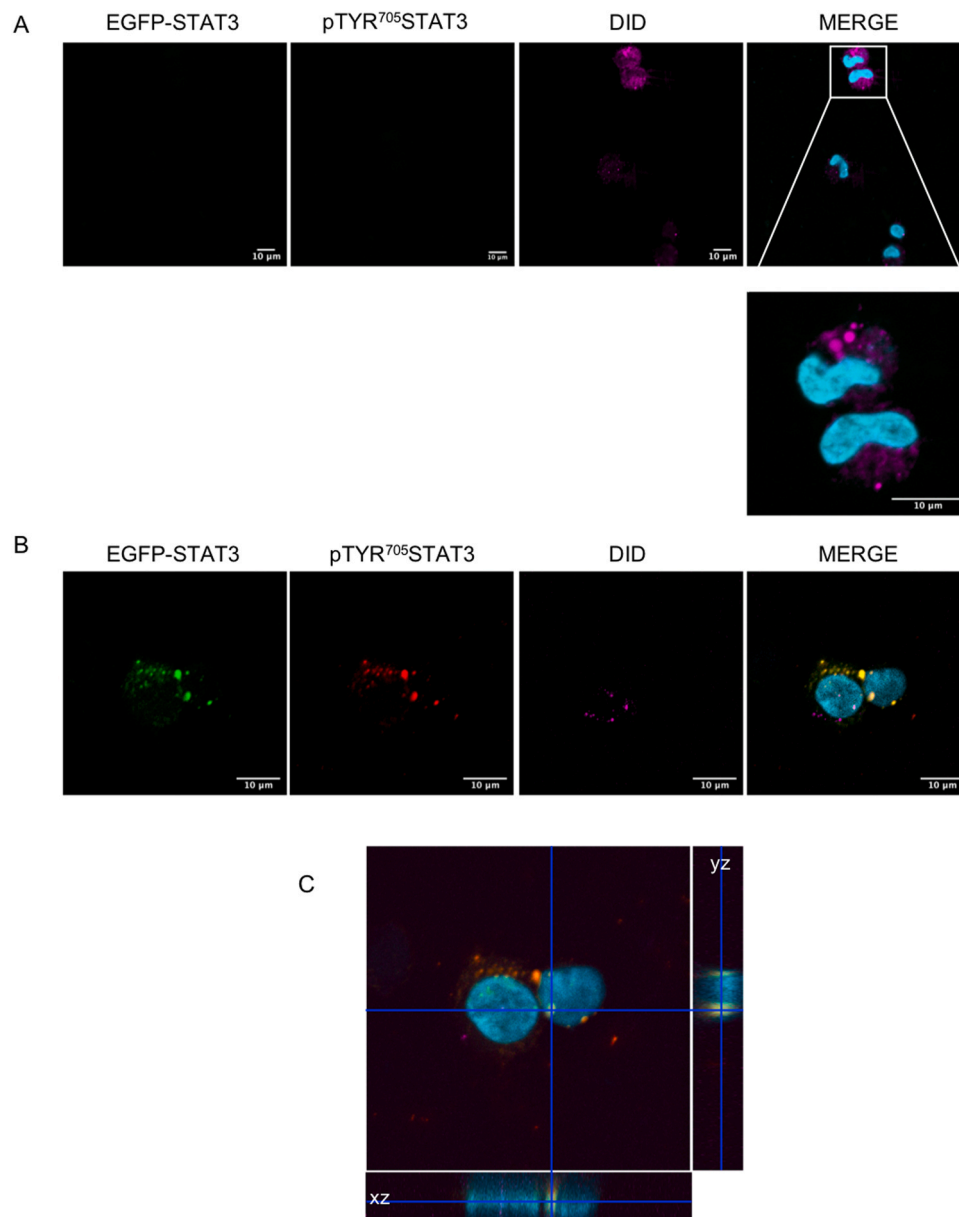
Fig. 10. Confocal microscopy of PBMCs treated with EGFP-STAT3 EVs. The cells were treated with unloaded and loaded EVs for 24 h and images were acquired by a confocal laser-scanning microscope using a 63 × objective lens. EGFP-STAT3 positive cells (green), pTYR^{705} STAT3 positive cells (red); DID-EVs (magenta); DAPI-nuclei (cyan). Scale bar 10 μm. (A) Representations of PBMCs after treatment with unloaded EVs. The zoom of merge shows that EVs are localized near nuclei. (B) Representations of PBMCs after treatment with EGFP-STAT3 EVs. The presence of co-localization of red and green signals in the merge images was highlighted in yellow. (C) The orthogonal sections (ZX and ZY) of merge image, shown in B, reveal that pTYR^{705}EGFP-STAT3 protein (yellow signal) is inside the nuclei (cyan signal). Images are representative of 3 different experiments.

Methodology, Funding acquisition. **Isacco Ferrarini:** Resources.

Declaration of Competing Interest

The authors report there are no competing interests to declare.

Availability of data

Data will be made available on request.

Acknowledgments

Appendix A. Supporting information

Supplementary data associated with this article can be found in the online version at doi:10.1016/j.nbt.2024.05.001.

References

[1] Raposo G, Stoorvogel W. Extracellular vesicles: exosomes, microvesicles, and friends. J Cell Biol 2013;200:373–83.

[2] van Niel G, D'Angelo G, Raposo G. Shedding light on the cell biology of extracellular vesicles. Nat Rev Mol Cell Biol 2018;19:213–28.

[3] Song X, Xue Y, Fan S, Hao J, Deng R. Lipopolysaccharide-activated macrophages regulate the osteogenic differentiation of bone marrow mesenchymal stem cells through exosomes. PeerJ 2022;10:e13442.

[4] Herrmann IK, Wood MJA, Fuhrmann G. Extracellular vesicles as a next-generation drug delivery platform. Nat Nanotechnol 2021;16:748–59.

[5] Cho E, Nam GH, Hong Y, Kim YK, Kim DH, Yang Y, et al. Comparison of exosomes and ferritin protein nanocages for the delivery of membrane protein therapeutics. J Control Release 2018;279:326–35.

[6] Ohno S, Takanashi M, Sudo K, Ueda S, Ishikawa A, Matsuyama N, et al. Systemically injected exosomes targeted to EGFR deliver antitumor microRNA to breast cancer cells. Mol Ther 2013;21:185–91.

[7] Pascucci L, Coccè V, Bonomi A, Ami D, Ceccarelli P, Ciusani E, et al. Paclitaxel is incorporated by mesenchymal stromal cells and released in exosomes that inhibit in vitro tumor growth: a new approach for drug delivery. J Control Release 2014; 192:262–70.

[8] Saari H, Lázaro-Ibáñez E, Viitala T, Vuorimaa-Laukkanen E, Siljander P, Yliperttula M. Microvesicle- and exosome-mediated drug delivery enhances the cytotoxicity of Paclitaxel in autologous prostate cancer cells. J Control Release 2015;220:727–37.

[9] Bagheri E, Abnous K, Farzad SA, Taghdisi SM, Ramezani M, Alibolandi M. Targeted doxorubicin-loaded mesenchymal stem cells-derived exosomes as a versatile platform for fighting against colorectal cancer. Life Sci 2020;261:118369.

[10] Didiot MC, Hall LM, Coles AH, Haraszti RA, Godinho BM, Chase K, et al. Exosome-mediated delivery of hydrophobically modified siRNA for Huntingtin mRNA silencing. Mol Ther 2016;24:1836–47.

[11] Morse MA, Garst J, Osada T, Khan S, Hobeika A, Clay TM, et al. A phase I study of dexosome immunotherapy in patients with advanced non-small cell lung cancer. J Transl Med 2005;3:9.

[12] Sun D, Zhuang X, Xiang X, Liu Y, Zhang S, Liu C, et al. A novel nanoparticle drug delivery system: the anti-inflammatory activity of curcumin is enhanced when encapsulated in exosomes. Mol Ther 2010;18:1606–14.

[13] Haney MJ, Klyachko NL, Zhao Y, Gupta R, Plotnikova EG, He Z, et al. Exosomes as drug delivery vehicles for Parkinson's disease therapy. J Control Release 2015;207: 18–30.

[14] He J, Shi J, Xu X, Zhang W, Wang Y, Chen X, et al. STAT3 mutations correlated with hyper-IgE syndrome lead to blockage of IL-6/STAT3 signalling pathway. J Biosci 2012;37:243–57.

[15] Woellner C, Gertz EM, Schaffer AA, Lagos M, Perro M, Glocker EO, et al. Mutations in STAT3 and diagnostic guidelines for hyper-IgE syndrome. J Allergy Clin Immunol 2010;125:424–32 [e428].

[16] Giacomelli M, Tamassia N, Moratto D, Bertolini P, Ricci G, Bertulli C, et al. SH2-domain mutations in STAT3 in hyper-IgE syndrome patients result in impairment of IL-10 function. Eur J Immunol 2011;41:3075–84.

[17] Heimall J, Davis J, Shaw PA, Hsu AP, Gu W, Welch P, et al. Paucity of genotype-phenotype correlations in STAT3 mutation positive Hyper IgE Syndrome (HIES). Clin Immunol 2011;139:75–84.

[18] Sundin M, Tesi B, Sund Bohme M, Bryceson YT, Putsep K, Chiang SC, et al. Novel STAT3 mutation causing hyper-IgE syndrome: studies of the clinical course and immunopathology. J Clin Immunol 2014;34:469–77.

[19] Levy DE, Darnell Jr JE. Stats: transcriptional control and biological impact. Nat Rev Mol Cell Biol 2002;3:651–62.

[20] Zhong Z, Wen Z, Darnell Jr JE. Stat3: a STAT family member activated by tyrosine phosphorylation in response to epidermal growth factor and interleukin-6. Science 1994;264:95–8.

[21] Darnell Jr JE. STATs and gene regulation. Science 1997;277:1630–5.

[22] Johnston PA, Grandis JR. STAT3 signaling: anticancer strategies and challenges. Mol Interv 2011;11:18–26.

[23] Kamimura D, Ishihara K, Hirano T. IL-6 signal transduction and its physiological roles: the signal orchestration model. Rev Physiol Biochem Pharm 2003;149:1–38.

[24] Bournazou E, Bromberg J. Targeting the tumor microenvironment: JAK-STAT3 signaling. JAKSTAT 2013;2:e23828.

[25] Butturini E, Carcereri de Prati A, Mariotto S. Redox regulation of STAT1 and STAT3 signaling. Int J Mol Sci 2020;21.

[26] Butturini E, Carcereri de Prati A, Boriero D, Mariotto S. Natural sesquiterpene lactones enhance chemosensitivity of tumor cells through redox regulation of STAT3 signaling. Oxid Med Cell Longev 2019;2019:4568964.

[27] Minegishi Y, Saito M, Tsuchiya S, Tsuge I, Takada H, Hara T, et al. Dominant-negative mutations in the DNA-binding domain of STAT3 cause hyper-IgE syndrome. Nature 2007;448:1058–62.

[28] Holland SM, DeLeo FR, Elloumi HZ, Hsu AP, Uzel G, Brodsky N, et al. STAT3 mutations in the hyper-IgE syndrome. N Engl J Med 2007;357:1608–19.

[29] Micsonai A, Moussong É, Wien F, Boros E, Vadászi H, Murvai N, et al. BeStSel: webserver for secondary structure and fold prediction for protein CD spectroscopy. Nucleic Acids Res 2022;50:W90–w98.

[30] Butturini E, Gotte G, Dell'Orco D, Chiavegato G, Marino V, Canetti D, et al. Intermolecular disulfide bond influences unphosphorylated STAT3 dimerization and function. Biochem J 2016;473:3205–19.

[31] Schulz E, Karagianni A, Koch M, Fuhrmann G. Hot EVs – how temperature affects extracellular vesicles. Eur J Pharm Biopharm 2020;146:55–63.

[32] Frank J, Richter M, de Rossi C, Lehr CM, Fuhrmann K, Fuhrmann G. Extracellular vesicles protect glucuronidase model enzymes during freeze-drying. Sci Rep 2018; 8:12377.

[33] Nkansah E, Shah R, Collie GW, Parkinson GN, Palmer J, Rahman KM, et al. Observation of unphosphorylated STAT3 core protein binding to target dsDNA by PEMSA and X-ray crystallography. FEBS Lett 2013;587:833–9.

[34] Butturini E, Darra E, Chiavegato G, Cellini B, Cozzolino F, Monti M, et al. S-Glutathionylation at Cys328 and Cys542 impairs STAT3 phosphorylation. ACS Chem Biol 2014;9:1885–93.

[35] Yang F, Moss LG, Phillips Jr GN. The molecular structure of green fluorescent protein. Nat Biotechnol 1996;14:1246–51.

[36] de Préval C, Hadam MR, Mach B. Regulation of genes for HLA class II antigens in cell lines from patients with severe combined immunodeficiency. N Engl J Med 1988;318:1295–300.

[37] Heinrich E, Hartwig O, Walt C, Kardani A, Koch M, Jahromi LP, et al. Cell-derived vesicles for antibiotic delivery-understanding the challenges of a biogenic carrier system. Small 2023:e2207479.

[38] Midekessa G, Godakumara K, Ord J, Viil J, Lättekivi F, Dissanayake K, et al. Zeta potential of extracellular vesicles: toward understanding the attributes that determine colloidal stability. ACS Omega 2020;5:16701–10.

[39] Beetler DJ, Di Florio DN, Bruno KA, Ikezu T, March KL, Cooper Jr LT, et al. Extracellular vesicles as personalized medicine. Mol Asp Med 2023;91:101155.

[40] Elliott RO, He M. Unlocking the power of exosomes for crossing biological barriers in drug delivery. Pharmaceutics 2021;13.

[41] Turano E, Scambi I, Virla F, Bonetti B, Mariotti R. Extracellular vesicles from mesenchymal stem cells: towards novel therapeutic strategies for neurodegenerative diseases. Int J Mol Sci 2023;24.

[42] Adli M. The CRISPR tool kit for genome editing and beyond. Nat Commun 2018;9: 1911.

[43] Scott B, Shen J, Nizzero S, Boom K, Persano S, Mi Y, et al. A pyruvate decarboxylase-mediated therapeutic strategy for mimicking yeast metabolism in cancer cells. Pharm Res 2016;111:413–21.

[44] Toward inflammation-free therapeutics in Alzheimer's disease. Nat Med. Vol. 28; 2022. p. 1765–6.

[45] Leader B, Baca QJ, Golan DE. Protein therapeutics: a summary and pharmacological classification. Nat Rev Drug Discov 2008;7:21–39.

[46] Fagagnini A, Pica A, Fasoli S, Montioli R, Donadelli M, Cordani M, et al. Onconase dimerization through 3D domain swapping: structural investigations and increase in the apoptotic effect in cancer cells. Biochem J 2017;474:3767–81.

[47] Yin L, Yuvienco C, Montclare JK. Protein based therapeutic agents: contemporary developments and challenges. Biomaterials 2017;134:91–116.

[48] Liu F, Wu X, Li L, Liu Z, Wang Z. Use of baculovirus expression system for generation of virus-like particles: successes and challenges. Protein Expr Purif 2013;90:104–16.

[49] Théry C, Witwer KW, Aikawa E, Alcaraz MJ, Anderson JD, Andriantsitohaina R, et al. Minimal information for studies of extracellular vesicles 2018 (MISEV2018): a position statement of the International Society for Extracellular Vesicles and update of the MISEV2014 guidelines. J Extra Vesicles 2018;7:1535750.

[50] Haney MJ, Klyachko NL, Harrison EB, Zhao Y, Kabanov AV, Batrakova EV. TPP1 delivery to lysosomes with extracellular vesicles and their enhanced brain distribution in the animal model of Batten disease. Adv Health Mater 2019;8: e1801271.

[51] Jiao Y, Tang Y, Li Y, Liu C, He J, Zhang LK, et al. Tumor cell-derived extracellular vesicles for breast cancer specific delivery of therapeutic P53. J Control Release 2022;349:606–16.

[52] Cvjetkovic A, Jang SC, Konečná B, Höög JL, Sihlbom C, Lässer C, et al. Detailed analysis of protein topology of extracellular vesicles-evidence of unconventional membrane protein orientation. Sci Rep 2016;6:36338.

[53] Rankin-Turner S, Vader P, O'Driscoll L, Giebel B, Heaney LM, Davies OG. A call for the standardised reporting of factors affecting the exogenous loading of extracellular vesicles with therapeutic cargos. Adv Drug Deliv Rev 2021;173: 479–91.